

Morphology control of metallic nanoparticles supported on carbon substrates in catalytic conditions

Y. Magnin ^{a, *}, E. Villermaux ^{a, b, c}, H. Amara ^{d, e}, C. Bichara ^f, R.J.M. Pellenq ^a

^a Multi-Scale Materials Science for Energy and Environment, The MIT / CNRS / Aix-Marseille University Joint Laboratory at Massachusetts Institute of Technology, Cambridge, MA, 02139, USA

^b Aix Marseille Université, CNRS, Centrale Marseille, IRPHE UMR 7342, Marseille, 13384, France

^c Institut Universitaire de France, Paris, 75005, France

^d Laboratoire d'Etude des Microstructures, ONERA-CNRS, UMR104, Université Paris-Saclay, BP 72, 92322, Châtillon Cedex, France

^e Université de Paris, Laboratoire Matériaux et Phénomènes Quantiques, CNRS, F-75013, Paris, France

^f Aix Marseille Univ, CNRS, CINAM, Marseille, France

ARTICLE INFO

Article history:

Received 9 October 2019

Received in revised form

9 December 2019

Accepted 10 December 2019

Available online 23 December 2019

Keywords:

Supported nanoparticles

Monte Carlo simulations

Tight binding

Carbon substrates

Atomic-scale modeling

ABSTRACT

Metallic nanoparticles are highly reactive objects, often used for their catalytic properties which strongly depend on their shape and morphology. Here we show that controlling the wetting properties on a substrate enables one to control the nanoparticle's shape, prevent their coalescence and maximize their surface reactivity. The highly ordered mesoporous carbon structures (CMK) are ideal to achieve such a control. CMK can be tuned during their synthesis and display convex and concave surfaces capable of modifying the wetting properties and the morphology of the nanoparticles incorporated. On a concave substrate, the nanoparticle tends to spread on the surface of the substrate resulting in a platelet particle shape, while on flat or convex ones, the nanoparticle shows a limited wetting behavior corresponding to a spherical shape. In addition, the carbon enrichment of the metallic nanoparticles in contact with CMK plays a key role in controlling their equilibrium morphology. This atomic scale study allows us to better understand the interaction between metal nanoparticles and CMK in order to master their morphology and improve their reactivity.

© 2019 Elsevier Ltd. All rights reserved.

1. Introduction

In the last decades, transition metal nanoparticles (NP) have become essential for various applications such as hydrocarbon reforming [1], chemical pollutant detectors [2], carbon nanotube (CNT) growth [3,4], catalysis [5] and other applications [6,7]. In this context, adjusting the size and shape of particles remains a challenge and is a crucial point since they can affect their performance as reported for catalytic applications [8–10]. A shape change can either modify the reactivity of particles by changing the ratio of coordinated/undercoordinated surface atoms, or by changing the size of edges and facets [10,11]. In the field of hydrogen storage, NP chemisorption, which consists in dissociating dihydrogen molecules at the surface or at interstitial positions inside a particle, is a good candidate because a large amount of hydrogen atoms in a

minimal host volume can be stored [12]. In addition, the size reduction of NP allows forming hydrides on different transition metals close to ambient pressure and temperature, with an enhanced adsorption/desorption kinetics [9,13] compared to the bulk counterpart. Indeed, the size reduction tends to increase the hydrogen solubility limit of a particle and decrease the enthalpy of hydride formation [14,15]. During particle synthesis or in a catalytic reaction, atoms that are a part of the feed or a part of substrate can be dissolved (such as C, H, O) into the particle. While heteroatoms as O and H can be desorbed at high temperature, the carbon enrichment of the particle can exist and thus change its surface electronic property [16,17] and in turn modifies the catalytic reaction. It has been shown that interstitial carbon atoms drive a selective hydrogenation of alkynes molecules [18,19], or significantly enhance hydrogen diffusion into the particle [20,21]. In all cases, one important limitation for chemisorption or other catalytic process, is the thermal stability of NP catalysts which tend to coalesce.

In this context, it has been revealed that highly ordered mesoporous carbons CMK can be used as wetting substrate [22] with

* Corresponding author.

E-mail address: magnin@mit.edu (Y. Magnin).

good performance for hydrogen storage or molecule adsorption [23–25]. CMK materials consist in a network of solid amorphous carbon cylinders (CMK-3) or empty carbon tubes (CMK-5), connected together by amorphous C cylindrical bars. Because of the CMK large porosity, gas molecules can be physisorbed at low temperature and controlled by the CMK pore size distribution [26]. In addition, when decorated by metallic NPs on their surface, CMK become interesting materials for chemisorption for two main reasons. First, the high porosity and topology of CMK can minimize the coalescence of the NPs, thanks to the large metal-carbon interaction and to the confinement effect [27]. Secondly, chemisorption can be tailored by changing the particle shape depending on the local curvature on the C structure which are of two types: a convex one on the outer tube surface and a concave one on the inner tube surface. It is interesting to note that both curvatures can be used to modify the NP shapes. However, because CMK structures are complex, it is difficult to get an insight in their role in the morphological control of catalysts. A deeper understanding at the atomic scale is required.

In this work, the interaction between CMK and NPs is studied by computer simulation in order to gain a better control of the morphology of the NPs and thus improve their catalytic properties. Before addressing the problem in all its complexity, we first focus on pristine carbon structures such as graphene and nanotubes, which have a flat surface (graphene) or convex/concave curvatures (CNT). These two structures are used as perfect synthetic carbon substrates in order to facilitate the understanding of the wetting mechanisms of NP and emphasized the effect of the substrate curvature. The CMK is then studied to see how the morphology of nanoparticles can be influenced by their interaction with such a more complex and realistic substrate. An important outcome of these calculations is to show that the carbon content inside the NP plays a crucial role by modifying the wetting properties and making it possible to tune the energy of the interface between the CMK and the catalyst. Indeed, we demonstrate that the thermal energy allows amorphous carbon atoms of CMKs to be dissolved into the metallic catalysts. This behavior was not observed for sp^2 carbon structures as graphene or nanotubes due to the strong carbon binding energy. However, for amorphous structures as CMK, a nanoparticle have a large enough solubility to dissolve sp carbons located at the surface of the CMK structure.

In order to simulate these systems, we used a tight-binding (TB) potential, which has proven efficient to accurately describe metal-carbon interactions for relatively large systems (here Ni-C). To describe the Ni-C system, we have developed a model based on the TB approximation, which provides an efficient tool to calculate carbon and transition-metal interactions [28], where only s , p electrons of C and d electrons of Ni are taken into account. Local densities of electronic states are calculated using a recursion method, where the first four continued fraction coefficients are only calculated exactly. The set of C-C, Ni-Ni and Ni-C TB interaction parameters used was shown to be transferable to different atomic configurations by comparison with *ab-initio* calculations or experimental data. In case of C-C interactions, parameters have been fitted to reproduce the competition between sp , sp^2 and sp^3 bonds. No van der Waals interactions are considered within this formalism. However, in the CMK, carbon bonds are mainly sp , sp^2 or sp^3 characters where our TB approach is perfectly adapted. Defects in carbon structures can also be investigated with our TB model as already discussed in Refs. [29,30]. Lastly, we can notice that in our simulations, the metallic NP tends to dewet carbon structures when increasing the carbon fraction dissolved in it. This is in qualitative agreement with experimental data, obtained by Naidich et al. [31], showing that the contact angle of a macroscopic Ni (and also Co and Fe) drop on graphite increases with the C fraction inside it. Such

wetting property is crucial to describe the physic in the present work. To conclude, all these results show how this TB potential is suitable for this study.

TB potential is implemented into a Monte Carlo algorithm (MC) in canonical (N_C, V, T) and grand canonical (μ_C, V, T) ensembles (GCMC). N_C is the number of C atoms, μ_C the carbon chemical potential, V the volume and T the temperature of the system. Such an approach combining a TB model and MC simulations is well suited to determine thermodynamic properties of Ni-C carbides. Applications of this model to the catalytic growth of graphene and carbon tubes have already been presented [32]. Simulations are performed on three different carbon substrates: graphene, carbon nanotubes and CMK. The metallic cluster used in simulations is a Wulff-shaped FCC NPs of few hundreds atoms (201, 405 and 807 Ni atoms depending on simulations). To investigate the wetting properties of metallic clusters on carbon substrates, the following procedure has been established. We first perform grand canonical calculations to simulate carbon dissolution in the catalyst. A serie of GCMC simulations have been performed at $T=1200\text{K}$ from a pure and isolated Ni nanoparticles (201, 405 and 807 atoms) for a set of μ_C ranging from -8 to -5 eV with a step of 0.5 eV. These simulations allow to determine the Ni-C isotherms and the equilibrium carbon concentration as a function of μ_C . Each run consists in 10^4 MC cycles to reach the equilibrium, where a MC cycle is defined as a displacement of each atoms of the structure. In each cycle, we performed 2500 displacement steps per atom and 1000 attempts were made to incorporate or to remove dissolved carbon atoms in the NP. Once the equilibrium is reached, a next 10^4 MC cycles was performed in order to average the number of C atoms absorbed inside NPs. In a second step, we introduce a carbon substrate (graphene, CNT, CMK) and we let the Ni-C NPs relaxed at $T=2000\text{K}$ during 10^3 MC cycles. The equilibrium shape a particle on the substrate curvature is then determined by performing simulated annealing. In this process the atomic configuration, initially at high temperature (2000 K), is slowly cooled down to 300 K, to ensure that the system is at any step as close as possible to the thermodynamic equilibrium. Typical runs consist in 4.10^6 MC cycles.

2. Results and discussion

2.1. Nanoparticles on a flat surface

Materials size reduction to the nanoscale has a strong impact on their properties as compared to their bulk counterpart. Indeed, below few nanometers, nanoparticle properties mainly depend on their surfaces than their limited volumes [33,34]. NP surfaces are responsible to an energy cost due to undercoordinated atoms that drives coalesce effects. However, when a pure metallic nanoparticle interacts with a carbon substrate, the covalent bonds formed between the p states of the carbon atoms and the valence d states of the metal [30,32] induce a wetting behavior of the particle on the substrate corresponding to a metal carbon interface. Particles are thus anchor to the substrate, limiting their diffusion behaviors. Metallic particles (Ni, Co, Fe, Pd, ...) can also present a carbon solubility that drive carbon atoms dissolution in interstitial positions in subsurface layers of a particle. This carbon feedstock comes from NP surrounding environment (precursor or substrate), that modify metal-carbon interfacial energy and in turn the wetting behavior. First, we seek to characterize the structural properties of a carbon-enriched nanoparticle. To do this, the phase diagram of Ni-C nanoparticles was calculated by GCMC simulations for system sizes up to about 3 nm. This study has already been published [34] and we only summarize the main conclusions below. In Fig. 1A, different phases are identified such as solid (S), liquid (L) or the segregation of carbon atoms on the surface of NP (SEG). In addition,

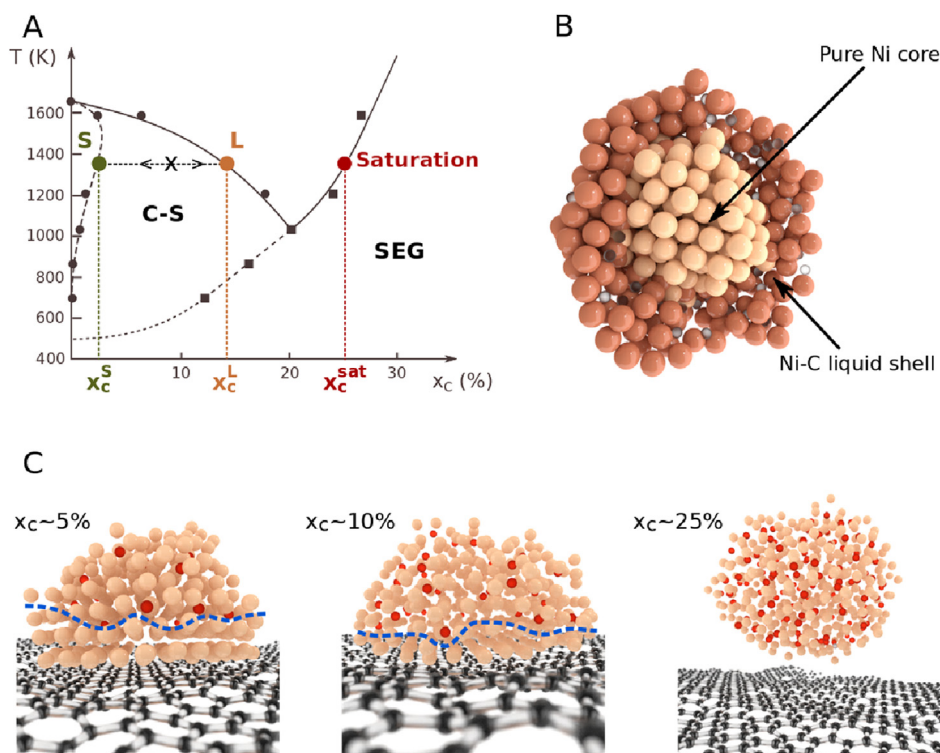


Fig. 1. A. Phase diagram of a 3 nm diameter Ni–C nanoparticle, corresponding to 807 Ni atoms. S, L and C–S correspond respectively to the solid, liquid and core-shell states, while SEG located above the limit of solubility, corresponds to the segregation states. B. Snapshot of a half Ni–C nanoparticle. Flush atoms correspond to well ordered Ni atoms in the core of the particle, while the brown sites correspond to the Ni–C disordered shell. C. Wetting behavior of a Ni–C nanoparticles (405 Ni atoms) on a graphene sheet for low, medium and high carbon concentrations. Below the blue dashed line the particle structure shows a pure and ordered Ni layers (flush) while above the blue line a disordered Ni–C structure can be seen with dissolved carbon atoms in red. (A colour version of this figure can be viewed online).

there is a core-shell state (C–S), where this stability domain connects the solid phase (S) to the liquid phase (L) through a heterogeneous continuum of core-shell states. As shown in Fig. 1B, this phase consists of a crystalline and nearly pure Ni core, containing a low carbon concentration x_c^S (solid concentration), surrounded by an Ni–C shell with a higher C concentration x_c^L (liquid concentration). Such a configuration is not observed in bulk. Indeed, it is a direct result of the nanoscale, where carbon atoms can diffuse inside the surface layers and induce partial melting of the NP surface.

We are now focusing on the interaction between nickel nanoparticles containing carbon atoms and graphene as a substrate. As already pointed out in Refs. [29,35], we notice that metallic nanoparticles tend to dewet from the graphene when the carbon fraction increases (see Fig. 1C). At low carbon concentration (x_c), the droplet shows a wetting angle (see Fig. S1 A in supplementary information), close to $\theta \sim 90^\circ$, corresponding a mildly wetting situation, while larger x_c favors a dewetting behavior, Fig. 2A. This is in qualitative agreement with experimental data, obtained by Naidich et al., showing that the contact angle of a macroscopic Ni (and also Co and Fe) drop on graphite increases with the C fraction dissolved inside [31]. It is interesting to note that due to its interaction with the substrate, the NP displays one or few pure crystalline Ni layers at the interface. Indeed, dissolved carbon atoms deplete the metal layers in the vicinity of graphene and remain in the upper layers, away from the substrate, Fig. 2B. This phenomenon has already been observed in the context of graphene growth by XPS experiments and computer simulations in the first metal layers of a Ni slab covered with an epitaxial graphene sheet [36,37]. When x_c increases, the dissolved carbon atoms populate the depleted metal layers. To maintain a constant liquidus concentration x_c^L , the number of ordered metal layers decreases and the remaining

volume occupied by dissolved C increases (as seen in Fig. 1C). This behavior induces a partial dewetting and lower NP/substrate adhesion. When the solubility limit ($x_c^{sat} \sim 25\%$) is reached, the nanoparticle is saturated by the carbon atoms and the work of adhesion goes to zero. As a result, the NP detached from the substrate, (as seen in Fig. 2C). The work of adhesion (Eq. (1)) can be calculated from the particle/substrate contact angle θ using the Young-Dupré equation (Eq. (2)).

$$W_{adh} = \gamma_{m-c} (1 + \cos \theta) \quad (1)$$

$$\cos \theta = -\frac{\gamma_{m-c} - \gamma_c}{\gamma_m(x_c)} \quad (2)$$

In (Eq. (2)), the NP surface energy corresponds to (γ_m), the metal-carbon interface energy by (γ_{m-c}) and the substrate surface energy by (γ_c).

Depending on the wetting behavior, a morphology change of the particle can be observed. At low carbon concentration on a flat substrate as graphene, the particle presents a half spherical shape, with a contact angle close to 90° . When x_c increases, the NP dewets and tends to a spherical shape with a minimal surface geometry, as seen in Fig. 3A. To understand this behavior, we develop simple arguments based on the system free energy. This expression is developed as a sum of the volume, surface and interfacial energies of a particle and its underlying substrate. Assuming that the volume of the NP is constant for all carbon concentrations, it is straightforward to show that the free energy minimization leads to the Young-Dupré equation. Details about the free energy minimization are given in the Supporting Information. In (Eq. (2)), the wetting angle between a NP supported on a flat substrate depends on the NP surface energy $\gamma_m(x_c)$, that is a function of the carbon concentration. When x_c

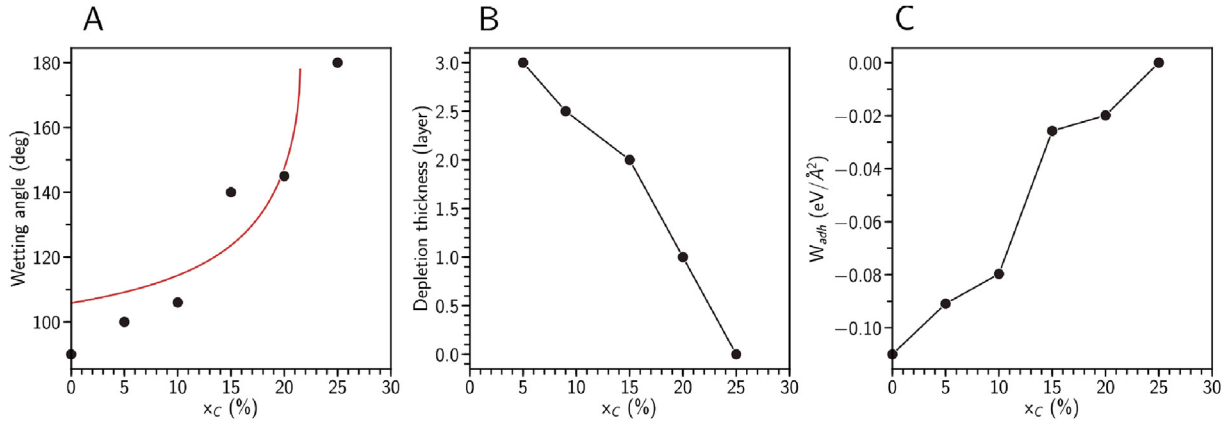


Fig. 2. A. Wetting angle, B. thickness of depleted carbon layers and C. the work of adhesion of a Ni nanoparticle supported on a graphene layer as a function of the carbon concentration dissolved into the particle. The red line in A corresponds to the wetting angle calculated from the Young-Dupré equation. (A colour version of this figure can be viewed online).

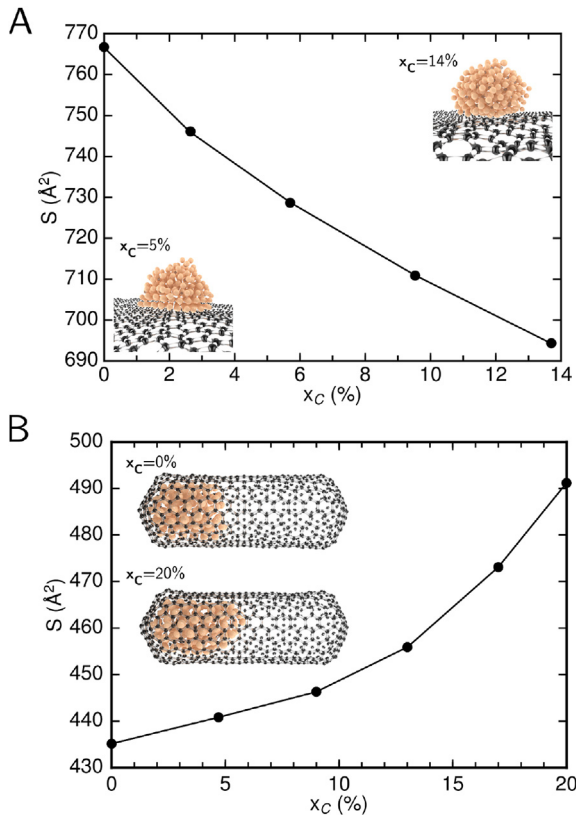


Fig. 3. A. Surface evolution of a Ni nanoparticle deposited on a graphene substrate as a function of the carbon concentration. B. Surface evolution of a Ni nanoparticle (201 Ni atoms), deposited on the inner surface of a single wall carbon nanotube, as a function of the carbon concentration. On a flat substrate (A), the nanoparticle shows a dewetting behavior when the carbon concentration increases. On a concave surface (B), the particle tends to spread on the substrate when the carbon concentration increases. All nanoparticles surfaces were determined using a convex hull algorithm. (A colour version of this figure can be viewed online).

increases, $\gamma_m(x_c)$ decreases. As a consequence, the particle favors the formation of a free surface and tends to lower the metal-carbon interface, resulting in a dewetting behavior. The final NPs geometry is thus impacted by the interplay of the particle-graphene interactions, the amount of carbon atoms dissolved inside the particle and the thermodynamical conditions of the system.

2.2. Nanoparticles inside carbon nanotube

The ability of a NP to sneak inside a CNT as in a fully wetting situation has been demonstrated both numerically [38,39] and experimentally [39,40]. During the growth of carbon nanotubes at moderate x_c , corresponding to the core-shell states described above, a partial wetting was observed. A fraction of metal atoms wets the inner tube surface, while the remaining metal atoms are located outside of the tube. At larger x_c , the nanoparticle does not wet anymore and interacts with the tube edge only, up to the detachment when the saturation is reached.

On a concave surface, such as the inner surface wall of a CNT, NP exhibits behavior opposite to that of graphene, Fig. 3B. For a low carbon concentration, the deviation from sphericity is minimal, corresponding to an encapsulated quasi-spherical NP. When the carbon concentration increases, the particle spreads along the axis of the tube. This effect is not so surprising at the low wetting limit ($\gamma_{m-c} > \gamma_m(x_c)$), with a wetting angle of $\theta > \pi/2$. For a sake of simplicity, the pore curvature is assimilated to a triangular groove with an half-angle at the top given by δ , (see Fig. S1 B in supplementary information). A simple calculation shows that the external surface A of a NP with a volume Ω elongated along the groove in the form of a bar, - denoted as a “slug”-, of length ℓ is approximately given by

$$A = 2 \frac{\Omega}{\ell} + 2\alpha \left(\frac{\Omega \ell}{f(\theta(x_c), \delta)} \right)^{1/2}, \quad (3)$$

$$\text{with } \alpha = \theta(x_c) + \delta - \pi/2, \quad (4)$$

$$\text{and } f(\theta(x_c), \delta) = \frac{\cos(\pi - \theta(x_c) - \delta) \sin(\theta(x_c) - \pi/2)}{\sin \delta} + \alpha. \quad (5)$$

The first term in A stands for the contribution of the extremities of the slug, and the second for the one of its cap. At equilibrium, corresponding to the free energy minimum given by (Eq. (2)), the surface area minimization $\partial A(x_c)/\partial \ell|_{\ell=\ell_\star} = 0$ at constant volume Ω , provides the optimal length ℓ_\star of the deformed NP as

$$\ell_\star \sim \left(\frac{\Omega}{\delta} \right)^{1/3}, \quad (6)$$

for small δ , demonstrating how a NP is more elongated in a groove with smaller angle δ . Hence, a spherical NP with diameter much

smaller than the radius of curvature of the surface on which it sits (i.e. $\delta \rightarrow \pi/2$) remains close to spherical, whereas when its diameter matches that of the tube to which it is attached (i.e. $\delta \rightarrow 0$), the NP deforms into an elongated slug, as suggested by Fig. 4A. In this case, the driving force to dissolve sp^2 carbon atoms from the substrate is too low. Therefore, the nanoparticle tends to elongate and form an interface with the substrate. When the radius of the NP is close to the one of the substrate, interface formation is favored due to the small difference between NP and CMK tube radius. In Fig. 4B, we show the particle length evolution as a function of wetting angles (θ, δ) using the complete form of equation (Eq. (5)) in relation (Eq. (3)). Interestingly, the elongation is mostly controlled by the apex angle δ and ranges from 2 nm corresponding to the diameter of an isolated nanoparticle to 5 nm for small angle δ .

2.3. Ordered mesoporous carbon CMK substrate

Beyond these simple geometries, we used an highly ordered mesoporous carbon CMK as wetting substrate [22]. CMK materials offer good mechanical and thermal stability, high pore volume, electrical conductivity and two curvatures (concave and convex). Monte Carlo simulations were performed with a CMK-5 structure, generated by Jain et al. [23], with a pure 2 nm diameter NP, initially deposited on two different locations. In the first case, the metallic NP lies at the edge of the CMK tube, in the second case it is on the outer tube surface. Note that the total number of atoms in the simulation is about 4000 atoms. In terms of calculation time, these simulations are very long and difficult to converge.

During the first 10^6 iterations, the system is relaxed at

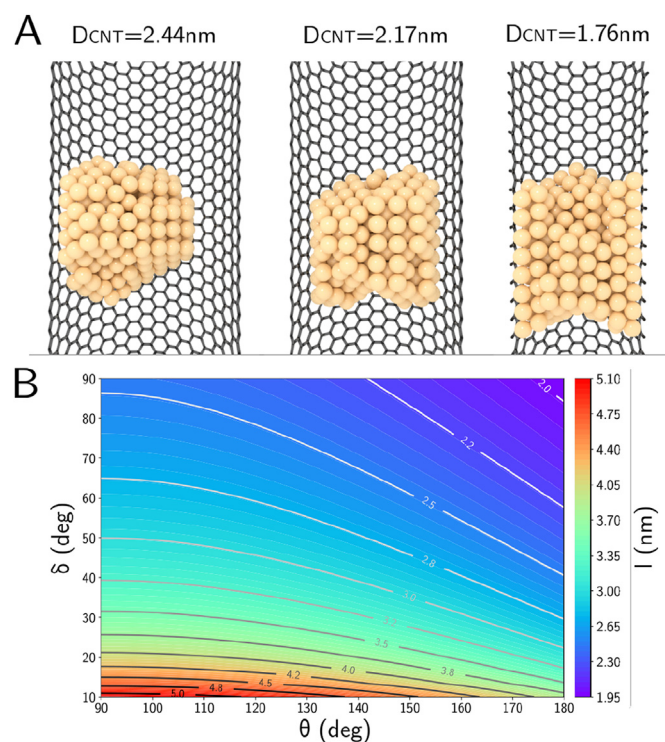


Fig. 4. A. Wetting behavior of a pure 2 nm Ni nanoparticle (201 Ni atoms), on the inner surface of single wall nanotubes with diameters corresponding respectively from the left to the right at $D_{CNT}=2.44, 2.17$ nm and 1.76 nm. Depending on diameter ratio of particle and tube, nanoparticles show different elongation depending on tube diameters. On small tube diameter, the particle shows a mostly platelet shape, while on large diameter tube, it shows an half spherical one. B. Map length of a particle wetting a curved surface as a function of the wetting angles θ and δ according to (Eq. (3)) and (Eq. (5)). (A colour version of this figure can be viewed online).

$T = 2000$ K. The next iterations correspond to an annealing from $T = 2000$ K–300 K.

As a first step, we consider the wetting behavior of a Ni NP on the inner tube surface of a CMK-5 to characterize the interaction with a concave surface. During the thermalization at $T = 2000$ K, the NP melts and penetrates inside the pore as seen in Fig. 6. This wetting behavior can be seen when the metallic particle contains a low or a moderate carbon concentration, corresponding to the core-shell states described above. In this case, the NP will favor metal-carbon interactions in order to heal metal atoms dangling bonds located at the surface of the particle. Thus, at high temperature the particle is in a liquid state and sneaks into the tube. While the temperature decreases, the lower part of the particle will crystallize and dissolved carbon atoms will diffuse to the upper part of the particle. This carbon depletion tends to increase the NP-substrate interaction as explain above (see Fig. 1).

In addition, if the curvature radius of the tube is in the same order than the NP, the metal-substrate interface will be increase for a small particle deformation. CMK pore diameters are usually around few nanometers. The wetting properties reported in this work could be different for larger NP where the carbon solubility should tends to the bulk around 10% instead of 25% for nanometer diameters [34]. We can thus imagine than large particle can only present a core shell state preventing the spreading effect inside tubular substrate. Interestingly, the analysis of the evolution of the carbon concentration within the particle shows an enrichment during this phase, to reach a maximum around $x_c \sim 8\%$, Fig. 5A. This carbon concentration remains constant throughout the cooling process from $T = 2000$ K–300 K. Actually, this behavior is directly related to the ability of the nanoparticle to dissolve sp carbon from the CMK. Indeed, sp carbon adatoms or short chains are present in the CMK structure, while, in the case of sp^2 structures (graphene and nanotube), such an effect has not been observed since C–C bonds are strong and not very reactive to the presence of the metal. The ability of a NP to poorly dissolve carbon sp bonds is shown on Fig. 5B, where the ratio of sp and sp^2 varies during the annealing process. From the high to the low temperature, the ratio of sp carbons decreases by 7%, while sp^2 carbon increases by 7%. Note that the thermal energy allows the NP to diffuse into the structure and remove some structural defects of the carbon structure. Moreover, the analysis in terms of local energy allows us to go further in understanding this phenomenon. Indeed, at the beginning of the simulation, the pure nanoparticle starts to dissolve carbon atoms, which results in an increasing energy of nickel located at the surface of the NP (in the vicinity of dissolved carbon). In parallel with this observation, it can be seen that the energy of Ni atoms in the layers depleted by carbon decreases drastically. As soon as the evolution of these two quantities crosses over, the nanoparticle no longer dissolves carbon and reach a maximum C concentration around $x_c \sim 8\%$, Fig. 5. Finally, it is interesting to note that at 300 K, the particle interacts strongly with the concave surface of the CMK, and tends to spread along the interface to increase its surface. Such a configuration is therefore favorable to promote catalytic processes by limiting coalescence effects. On the other hand, the interaction of NP with convex surfaces is less favorable in this respect. Here again, we observe an enrichment of the particle in carbon with a melted NP at high temperature. However, as can be seen from the evolution of the surface as a function of temperature, the contact surface is much smaller at low temperatures than for a concave surface.

3. Conclusion

In the present study, we have shown that the porous structure of CMKs is a playground that allow to modify the morphology of

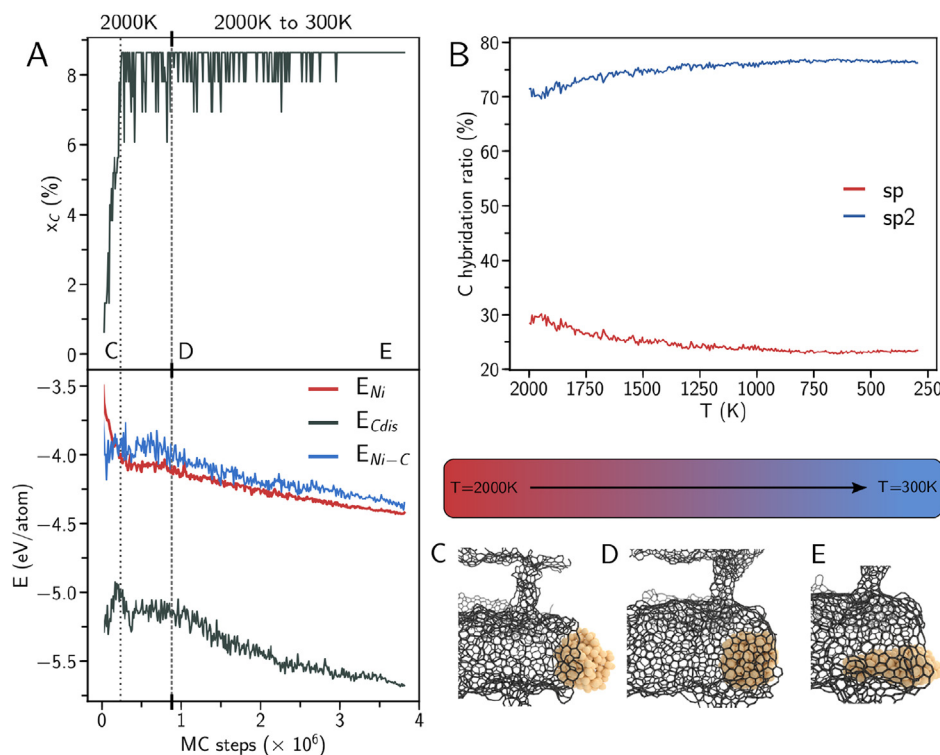


Fig. 5. A. (Upper panel) Monte Carlo time evolution of the carbon concentration dissolved into a 2 nm diameter metallic nanoparticle (201 Ni atoms). (Lower panel) Monte Carlo step evolution of energies for Ni (E_{Ni}), C (E_{Cdis}) and Ni surrounded by dissolved C atoms (E_{Ni-C}). B. Evolution of the sp and sp² hybridization ratio in CMK as a function of the temperature during the annealing. C-E. Snapshots corresponding to the system evolution as a function of the temperature. C. The nanoparticle interacts with the tube edge of the CMK. C. The nanoparticle wets the inner tube surface of the CMK. D. Slug configuration after annealing. (A colour version of this figure can be viewed online).

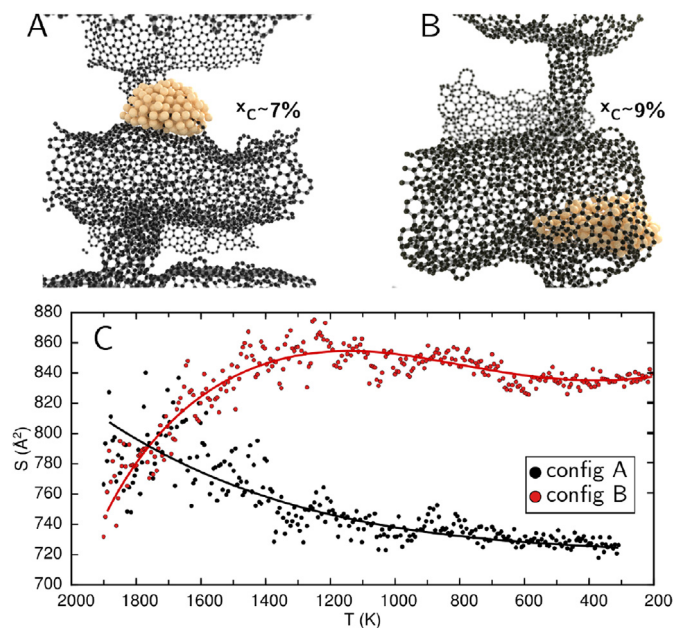


Fig. 6. A. Wetting behavior of a nanoparticle at the top of a CMK-5 tube (convex surface). B. Wetting behavior of a nanoparticle on the inner CMK-5 tube (concave surface). C. Nanoparticle surface evolution of cases (A) and (B) during annealing from $T = 2000\text{K} - 300\text{K}$. (A colour version of this figure can be viewed online).

nanoparticles. It is thus possible to take advantage of this complex carbon architecture to deposit nanoparticles on concave and convex contact areas while enriching the particle with carbon. It

then becomes possible to modify their wetting properties which are directly related to the local curvature of the substrate, but also to the ability of the metal catalyst to dissolve carbon from the CMK. A Ni nanoparticle is covalently bonded to the carbon substrate, ensuring a strong adhesion energy between both materials. However, the particle-substrate interaction depends on the interstitial carbon fraction dissolved into the NP. When x_c increases, the adhesion energy decreases up to the detachment at a carbon concentration corresponding to the saturation. On a flat or convex substrate the NP shows a limited wetting behavior resulting in an almost spherical shape. For concave substrates and when the curvature radius of both NP and substrate are of the same order, the NP is allowed to maximize the metal-carbon interface resulting in NP spreading. Thus, the carbon-enriched NP seeks to maximize its surface area with the substrate, limiting its ability to coalesce. Such a morphology is therefore a real advantage for stability of supported particle in catalytic applications. Furthermore, different experimental studies have shown that carbon-enriched NPs can enhance catalytic properties. This has recently been shown in the case of Mg [20] and Pd [18] NPs containing carbon atoms. It can be noted that these results for nickel can be easily extended and generalized to other catalysts that also have the ability to dissolve carbon and form carbide nanoparticles. On this last point, we should notice that a very promising chemical synthesis technique of transition metal carbide nanoparticles has been developed to produce a wide range of homogeneous nanoparticles with controlled stoichiometry and sizes [41]. Our study therefore provides valuable and unique details on the wetting mechanisms of metal nanoparticles supported on carbon substrate at the nanoscale and represents a major step forward in their use for many applications.

Declaration of competing interest

The authors declare that they have no known competing financial interests or personal relationships that could have appeared to influence the work reported in this paper.

Acknowledgement

Y. Magnin gratefully acknowledges the UCP, Computational Center of the Cergy-Pontoise University for the CPU time used to perform numerical simulations.

Appendix A. Supplementary data

Supplementary data to this article can be found online at <https://doi.org/10.1016/j.carbon.2019.12.025>.

References

- [1] R. Benrabaa, A. Löfberg, A. Rubbens, E. Bordes-Richard, R.N. Vannier, A. Barama, Structure, reactivity and catalytic properties of nanoparticles of nickel ferrite in the dry reforming of methane, *Catal. Today* 203 (2013) 188–195, <https://doi.org/10.1016/j.cattod.2012.06.002>. URL
- [2] N. Moghimi, M. Mohapatra, K.T. Leung, Bimetallic nanoparticles for arsenic detection, *Anal. Chem.* 87 (11) (2015) 5546–5552, <https://doi.org/10.1021/ac504116d>.
- [3] R. Rao, C.L. Pint, A.E. Islam, R.S. Weatherup, S. Hofmann, E.R. Meshot, F. Wu, C. Zhou, N. Dee, P.B. Amama, J. Carpena-Núñez, W. Shi, D.L. Plata, E.S. Penev, B.I. Yakobson, P.B. Balbuena, C. Bichara, D.N. Futaba, S. Noda, H. Shin, K.S. Kim, B. Simard, F. Mirri, M. Pasquali, F. Fornasiero, E.I. Kauppinen, M. Arnold, B.A. Cola, P. Nikolaev, S. Arepalli, H.M. Cheng, D.N. Zakharov, E.A. Stach, J. Zhang, F. Wei, M. Terrones, D.B. Geohegan, B. Maruyama, S. Maruyama, Y. Li, W.W. Adams, A.J. Hart, Carbon nanotubes and related nanomaterials: critical advances and challenges for synthesis toward mainstream commercial applications, *ACS Nano* 12 (12) (2018) 11756–11784, <https://doi.org/10.1021/acsnano.8b06511>.
- [4] Y. Magnin, H. Amara, F. Ducastelle, A. Loiseau, C. Bichara, Entropy-driven stability of chiral single-walled carbon nanotubes, *Science* 362 (6411) (2018) 212–215, <https://doi.org/10.1126/science.aat6228>, arXiv:<https://science.sciencemag.org/content/362/6411/212.full.pdf>, <https://science.sciencemag.org/content/362/6411/212>.
- [5] L. Wang, R.T. Yang, Hydrogen storage properties of carbons doped with ruthenium, platinum, and nickel nanoparticles hydrogen storage properties of carbons doped with ruthenium, platinum, and nickel nanoparticles, *J. Phys. Chem. C* 112 (2008) 12486–12494, <https://doi.org/10.1021/jp803093w>.
- [6] A.Z. Moshfegh, Nanoparticle catalysts, *J. Phys. D Appl. Phys.* 42 (23) (2009) 233001, <https://doi.org/10.1088/0022-3727/42/23/233001>.
- [7] L. Schlappbach, A. Züttel, For mobile applications, *Nature* 414 (November) (2001) 353–358, <https://doi.org/10.1038/35104634>. URL, <http://www.ncbi.nlm.nih.gov/pubmed/11713542>.
- [8] A. Cho, Connecting the dots to custom catalysis, *Science* 299 (March) (2003) 1684.
- [9] C. Zlotea, M. Lacroche, Role of nanoconfinement on hydrogen sorption properties of metal nanoparticles hybrids, *Colloid. Surf. Physicochem. Eng. Asp.* 439 (2013) 117–130, <https://doi.org/10.1016/j.colsurfa.2012.11.043>. URL, <http://www.sciencedirect.com/science/article/pii/S0927775712008151>.
- [10] S. Mostafa, F. Behafarid, J.R. Croy, L.K. Ono, L. Li, J.C. Yang, A.I. Frenkel, B.R. Cuenya, Shape-Dependent catalytic properties of Pt Nanoparticles.pdf, *J. Am. Chem. Soc.* 132 (2010) 15714–15719.
- [11] R. Xu, D. Wang, J. Zhang, Y. Li, Shape-dependent catalytic activity of silver nanoparticles for the oxidation of styrene, *Chem. Asian J.* 1 (6) (2006) 888–893, <https://doi.org/10.1002/asia.200600260>.
- [12] A. Züttel, Hydrogen storage methods, *Naturwissenschaften* 91 (4) (2004) 157–172, <https://doi.org/10.1007/s00114-004-0516-x>.
- [13] H. Reardon, J.M. Hanlon, R.W. Hughes, A. Godula-Jopek, T.K. Mandal, D.H. Gregory, Emerging concepts in solid-state hydrogen storage: the role of nanomaterials design, *Energy Environ. Sci.* 5 (3) (2012) 5951–5979, <https://doi.org/10.1039/c2ee03138h>.
- [14] J. Sarkar, S. Bhattacharyya, Application of graphene and graphene-based materials in clean energy-related devices Minghui, *Arch. Therm.* 33 (4) (2012) 23–40, <https://doi.org/10.1002/er>, arXiv:[arXiv:1011.1669v3](https://arxiv.org/abs/1011.1669v3).
- [15] T.P. Senftle, M.J. Janik, A.C. Van Duin, A ReaxFF investigation of hydride formation in palladium nanoclusters via Monte Carlo and molecular dynamics simulations, *J. Phys. Chem. C* 118 (9) (2014) 4967–4981, <https://doi.org/10.1021/jp411015a>.
- [16] H. Bluhm, M. Hävecker, A. Knop-Gericke, E. Kleimenov, R. Schlögl, D. Teschner, V.I. Bukhtiyarov, D.F. Ogletree, M. Salmeron, Methanol oxidation on a copper catalyst investigated using in situ X-ray photoelectron spectroscopy, *J. Phys. Chem. B* 108 (38) (2004) 14340–14347, <https://doi.org/10.1021/jp040080j>.
- [17] R. Blume, M. Hävecker, S. Zafeirotos, D. Teschner, E. Vass, P. Schnörch, A. Knop-Gericke, R. Schlögl, S. Lizzit, P. Dudin, A. Barinov, M. Kiskinova, Monitoring in situ catalytically active states of Ru catalysts for different methanol oxidation pathways, *Phys. Chem. Chem. Phys.* 9 (27) (2007) 3648–3657, <https://doi.org/10.1039/b700986k>.
- [18] D. Teschner, J. Borsodi, A. Wootsch, Z. Révay, M. Hävecker, A. Knop-Gericke, S.D. Jackson, R. Schlögl, The roles of subsurface carbon and hydrogen in palladium-catalyzed alkyne hydrogenation, *Science* 320 (5872) (2008) 86–89, <https://doi.org/10.1126/science.1155200>.
- [19] J.J. Velasco-Vélez, D. Teschner, F. Girgsdies, M. Hävecker, V. Streibel, M.G. Willinger, J. Cao, M. Lamoth, E. Frei, R. Wang, A. Centeno, A. Zurutuza, S. Hofmann, R. Schlögl, A. Knop-Gericke, The role of adsorbed and subsurface carbon species for the selective alkyne hydrogenation over a Pd-black catalyst: an operando study of bulk and surface, *Top. Catal.* 61 (20) (2018) 2052–2061, <https://doi.org/10.1007/s11244-018-1071-6>. URL
- [20] A.J. Du, S.C. Smith, X.D. Yao, G.Q. Lu, Catalytic effects of subsurface carbon in the chemisorption of hydrogen on a Mg(0001) surface: an ab-initio study, *J. Phys. Chem. B* 110 (4) (2006) 1814–1819, <https://doi.org/10.1021/jp055972d>.
- [21] P. Adelhelm, P.E. De Jongh, The impact of carbon materials on the hydrogen storage properties of light metal hydrides, *J. Mater. Chem.* 21 (8) (2011) 2417–2427, <https://doi.org/10.1039/c0jm02593c>.
- [22] R. Ryoo, S.H. Joo, S. Jun, Synthesis of highly ordered carbon molecular sieves via template-mediated structural transformation, *J. Phys. Chem. B* 103 (37) (1999) 7743–7746, <https://doi.org/10.1021/jp991673a>.
- [23] S.K. Jain, R.J. Pellenq, K.E. Gubbins, X. Peng, Molecular modeling and adsorption properties of ordered silica-templated MCM mesoporous carbons, *Langmuir* 33 (9) (2017) 2109–2121, <https://doi.org/10.1021/acs.langmuir.6b04169>.
- [24] D. Kim, H. Kang, H. Park, S. Park, J.C. Park, K.H. Park, Nickel nanoparticles supported on CMK-3 with enhanced catalytic performance for hydrogenation of carbonyl compounds, *Eur. J. Inorg. Chem.* 21 (2016) (2016) 3469–3473, <https://doi.org/10.1002/ejic.201600318>.
- [25] S. Giraudet, Z. Zhu, Hydrogen adsorption in nitrogen enriched ordered mesoporous carbons doped with nickel nanoparticles, *Carbon* 49 (2) (2011) 398–405, <https://doi.org/10.1016/j.carbon.2010.09.035>. URL
- [26] T. Ohkubo, J. Miyawaki, K. Kaneko, R. Ryoo, N.A. Seaton, Adsorption properties of templated mesoporous carbon (CMK-1) for nitrogen and supercritical methane - experiment and GCMC simulation, *J. Phys. Chem. B* 106 (25) (2002) 6523–6528, <https://doi.org/10.1021/jp0200369>.
- [27] A. Schneemann, J.L. White, S. Kang, S. Jeong, L.F. Wan, E.S. Cho, T.W. Heo, D. Prendergast, J.J. Urban, B.C. Wood, M.D. Allendorf, V. Stavila, Nanostructured metal hydrides for hydrogen storage, *Chem. Rev.* 118 (22) (2018) 10775–10839, <https://doi.org/10.1021/acs.chemrev.8b00313>.
- [28] H. Amara, J.M. Roussel, C. Bichara, J.P. Gaspard, F. Ducastelle, Tight-binding potential for atomistic simulations of carbon interacting with transition metals: application to the Ni-C system, *Phys. Rev. B* 79 (1) (2009), 014109, <https://doi.org/10.1103/PhysRevB.79.014109>.
- [29] M. Diarra, A. Zappelli, H. Amara, F. Ducastelle, C. Bichara, Importance of carbon solubility and wetting properties of nickel nanoparticles for single wall nanotube growth, *Phys. Rev. Lett.* 109 (18) (2012) 185501, <https://doi.org/10.1103/PhysRevLett.109.185501>.
- [30] S. Karoui, H. Amara, C. Bichara, F. Ducastelle, Nickel-assisted healing of defective graphene, *ACS Nano* 4 (10) (2010) 6114–6120, <https://doi.org/10.1021/nn101822s>, PMID: 20929241.
- [31] Y. Naidich, V. Pevertailo, Wetting of graphite by nickel affected by the liquid-phase dissolution process of carbon, *Powder Metall. Met. Ceram.* 1 (97) (1971) 45–47.
- [32] H. Amara, C. Bichara, Modeling the growth of single-wall carbon nanotubes, *Top. Curr. Chem.* 375 (3) (2017) 55, <https://doi.org/10.1007/s41061-017-0141-8>.
- [33] P. Buffat, J.-P. Borel, Size effect on the melting temperature of gold particles, *Phys. Rev. A* 13 (1976) 2287–2298, <https://doi.org/10.1103/PhysRevA.13.2287>. URL, <https://link.aps.org/doi/10.1103/PhysRevA.13.2287>.
- [34] Y. Magnin, A. Zappelli, H. Amara, F. Ducastelle, C. Bichara, Size dependent phase diagrams of nickel-carbon nanoparticles, *Phys. Rev. Lett.* 115 (20) (2015) 205502, <https://doi.org/10.1103/PhysRevLett.115.205502>.
- [35] J.M. Aguiar-Hualde, Y. Magnin, H. Amara, C. Bichara, Probing the role of carbon solubility in transition metal catalyzing single-walled carbon nanotubes growth, *Carbon* 120 (2017) 226–232.
- [36] A. Benayad, X.S. Li, Carbon free nickel subsurface layer tessellating graphene on Ni(111) surface, *J. Phys. Chem. C* 117 (9) (2013) 4727–4733, <https://doi.org/10.1021/jp312760z>.
- [37] R.S. Weatherup, H. Amara, R. Blume, B. Dlubak, B.C. Bayer, M. Diarra, M. Bahri, A. Cabrero-Vilatela, S. Caneva, P.R. Kidambi, M.-B. Martin, C. Deranlot, P. Seneor, R. Schloegl, F. Ducastelle, C. Bichara, S. Hofmann, Interdependency of subsurface carbon distribution and graphene - catalyst interaction, *J. Am. Chem. Soc.* 136 (111) (2014) 13698–13708, <https://doi.org/10.1021/ja505454v>.
- [38] M. He, Y. Magnin, H. Amara, H. Jiang, H. Cui, F. Fossard, A. Castan, E. Kauppinen, A. Loiseau, C. Bichara, Linking growth mode to lengths of single-walled carbon nanotubes, *Carbon* 113 (2017) 231–236, <https://doi.org/10.1016/j.carbon.2016.11.057>.
- [39] M. He, Y. Magnin, H. Jiang, H. Amara, E. Kauppinen, A. Loiseau, C. Bichara,

- Growth modes and chiral selectivity of single-walled carbon nanotubes, *Nanoscale* (2018) 6744–6750, <https://doi.org/10.1039/C7NR09539B>, arXiv: arXiv:1802.04029v1, <http://pubs.rsc.org/en/Content/ArticleLanding/2018/NR/C7NR09539B>.
- [40] A.S. Andreev, a.A. Kazakova, A.V. Ishchenko, A.G. Selyutin, O.B. Lapina, V.L. Kuznetsov, J.B. d'Espinose de Lacaillerie, Magnetic and dielectric properties of carbon nanotubes with embedded cobalt nanoparticles, *Carbon* 114 (2017) 39–49, <https://doi.org/10.1016/j.carbon.2016.11.070>.
- [41] D. Ressnig, S. Moldovan, O. Ersen, P. Beaunier, D. Portehault, C. Sanchez, S. Carencu, An expeditious synthesis of early transition metal carbide nanoparticles on graphitic carbons, *Chem. Commun.* 52 (61) (2016) 9546–9549, <https://doi.org/10.1039/c6cc04157d>.